Journal of the European Ceramic Society 39 (2019) 212–221

Contents lists available at ScienceDirect

Journal of the European Ceramic Society

journal homepage: www.elsevier.com/locate/jeurceramsoc

Original Article

Characterization and application of a novel low viscosity polysilazane for the manufacture of C- and SiC-fiber reinforced SiCN ceramic matrix composites by PIP process

Bernd Mainzer[a], Chaorong Lin[b], Raouf Jemmali[a], Martin Frieß[a,*], Ralf Riedel[b], Dietmar Koch[a]

[a] Deutsches Zentrum für Luft- und Raumfahrt e.V. (DLR), Institut für Bauweisen und Strukturtechnologie, Pfaffenwaldring 38-40, 70569, Stuttgart, Germany
[b] Technische Universität Darmstadt, Institut für Materialwissenschaft, Otto-Berndt-Str. 3, 64287, Darmstadt, Germany

ARTICLE INFO

Keywords:
SiC/SiCN
C/SiCN
Polysilazane
PIP
Interface

ABSTRACT

Four unidirectional fiber reinforced SiCN ceramic matrix composites were manufactured by means of polymer infiltration and pyrolysis. Two carbon fibers (T800H and Granoc XN90) as well as two silicon carbide fibers (Tyranno ZMI and SA3) without fiber coating were chosen. As matrix precursor, a poly(methylvinyl)silazane was investigated and utilized. The composites with the SA3 and the XN90 fiber had the highest tensile strengths of 478 and 288 MPa, respectively. It is considered that these high modulus fibers with the low modulus SiCN matrix create weak matrix composites. After exposure to air (T = 1200 °C, 10 h), a significant decrease of the mechanical properties was found, caused by the burnout of carbon fibers and the oxidation through open pores stemming from the PIP process and SiCN/SiCN interfaces in case of the SiC fiber based composites.

1. Introduction

Non-oxide ceramic matrix composites (CMCs) exhibit high specific strength at elevated temperatures as well as a high fracture strain and thermal shock resistance [1–3]. The application of such composites is highly dependent from the chosen fiber. Carbon fiber reinforced CMCs, like C/SiC usually are developed for friction applications as well as short time applications such as nozzles or thermal protection systems for aerospace vehicles [4–6]. Due to the oxidation sensitivity of carbon fibers, these composites are not regarded for long-time applications in high-temperature oxidative environments. In order to overcome this drawback, silicon carbide fiber reinforced composites were developed in the past 30 years. Such composites, like SiC/SiC have found application in jet engines as shroud material and are of high interest for next generation nuclear reactors [7–11].

Usually fiber coatings such as pyrolytic carbon (pyC) or boron nitride are applied in order to create a weak interphase and thereby to achieve damage tolerant, high strength composites [12–15]. The three most common routes to infiltrate the matrix of non-oxide CMCs are polymer infiltration and pyrolysis (PIP), chemical vapor infiltration (CVI) and liquid silicon infiltration (LSI). The PIP process is based on the infiltration of preceramic silicon-based organo-substituded polymers such as polysiloxanes, polycarbosilanes or polysilazanes into fiber prepregs and subsequent pyrolysis [16]. Thereby, the precursor is transformed by decomposition to an amorphous or crystalline ceramic, depending on the chosen temperature. In case of polysilazanes, either an amorphous silicon carbonitride or a crystalline SiC/Si_3N_4 composite matrix can be achieved [17–19]. The decomposition during pyrolysis leads to a volume shrinkage of the polymer and to the formation of porosity. The repetition of the PIP cycle leads to reduced porosities.

This work focusses on several aspects of the development of low-cost PIP-CMCs: An experimental low viscous poly(methylvinyl)silazane is utilized for the first time for the manufacture of fiber reinforced CMCs. Due to the found obstacles regarding infiltration and control of the curing step of polysilazanes, the applicability and influence of dicumyl peroxide as curing agent on various properties of the polysilazane is investigated. Besides the improvement of the manufacturing process, this work evaluates different fiber/SiCN combinations, especially in order to find systems with high tensile strength without using an additional fiber coating. Moreover, the oxidation resistance of these CMCs at 1200 °C is investigated. For the application in jet engines, such CMCs are equipped with additional environmental barrier coatings [7]. Since CVD-SiC coatings have proven to successfully protect in-house manufactured C/C-SiC composites under re-entry conditions, combustion chamber conditions or utilized as nozzle extension, half of the manufactured SiCN based composites were coated with CVD-SiC and compared to those without coating [4,20,21].

* Corresponding author.
E-mail address: martin.friess@dlr.de (M. Frieß).

https://doi.org/10.1016/j.jeurceramsoc.2018.09.042
Received 28 June 2018; Received in revised form 3 September 2018; Accepted 25 September 2018
Available online 27 September 2018
0955-2219/

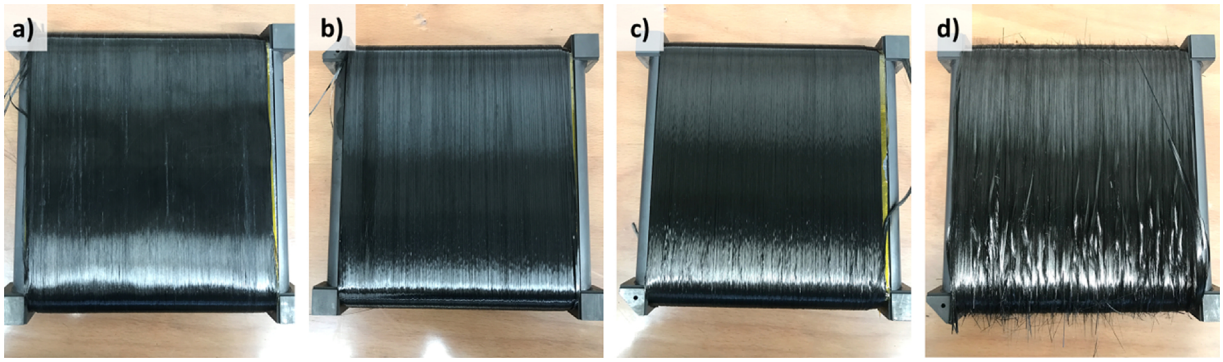

Fig. 1. UD fiber preforms wound on graphite mandrels: a) Tyranno ZMI; b) Tyranno SA3; c) T800H; d) XN90. The preform with XN90 fibers shows a considerable amount of damage.

2. Experimental procedure

2.1. CMC manufacturing

Unidirectional (UD) fiber reinforced composites were manufactured by means of polymer infiltration and pyrolysis (PIP). The UD preforms were created via filament winding on graphite mandrels (Fig. 1). A total of four different types of fibers, two silicon carbide and two carbon fibers were chosen (Table 1). The winding was performed with a winding angle of ± 0.38° for the Tyranno ZMI, Tyranno SA3 and T800H fiber. For the thicker tow of the Granoc XN90, a winding angle ± 1° was used. As matrix precursor, an experimental low viscous poly(methylvinyl)silazane denoted as PSZ10 (Fig. 2a, Clariant SE, Germany) was chosen. This precursor is a low molecular fraction of the commercially available polysilazane HTT1800. A total of 8 PIP cycles were performed with a mixture of the polysilazane and 1 wt.-% of dicumyl peroxide (DCP, Fig. 2b (Alfa Aesar, Germany)). The wound mandrels were infiltrated by means of resin transfer molding. Spacer plates were used in order to define the thickness and surface shape of the composites. The curing was performed at 260 °C for 4 h at a pressure of 20 bar in a nitrogen atmosphere. The pyrolysis was performed at 1300 °C at a pressure of 1 bar in a nitrogen atmosphere, too (HT1800GT, Linn High Therm GmbH, Germany). Each mandrel yielded in two 125 × 125 mm^2 plates which were grinded and cut into samples of 120 × 7 x 2.5 mm^3 for tensile tests. Half of the samples were coated with SiC by means of chemical vapor deposition (Schunk Group GmbH, Germany).

2.2. Characterization methods

Porosity values of the composites were determined by the Archimedes method (according to DIN EN 993-1). Their Young's moduli were determined with the strain rates from strain gauges. Half of the samples were oxidized in air at 1200 °C for 10 h. For each type of composite, 5 tensile samples were tested, in total 80 samples. The microstructures were investigated by means of SEM (Zeiss Ultra Plus, Carl Zeiss Microscopy GmbH, Germany) at a voltage of 5 kV. The images of fractured surfaces were made with the SE2 detector, those of polished surfaces with the In-Lens detector. The pore structures were investigated by means of µCT (nanotom, GE Sensing & Inspection Technologies GmbH, Germany) with a 12-bit flat panel detector with an active area of 2348 × 2348 pixels with 50 microns per pixel. The CT scans were performed with the X-ray parameters 80 kV/180 µA at an exposure time of 1000 ms.

Since 1 wt.-% dicumyl peroxide was used for the manufacture of the CMCs, its influence on various properties was investigated. The viscosity was determined in air by an oscillatory measurement with $f = 10\,s^{-1}$ and $\Phi = 0.01°$ in a plate/plate rheometer system from 25 to 300 °C with a heating rate of 2 K/min (MCR302, Anton Paar GmbH, Austria). In order to simulate curing in the resin transfer molding process, differential scanning calorimetry was made in gold plated high pressure capsules (Netzsch DSC 404, Netzsch Gerätebau GmbH, Germany). The same temperature range and heating rate were chosen for comparison. Infrared spectroscopy was performed on a Vertex 70 FT-IR (Bruker, USA). Thermogravimetric measurements were made to analyze the degassing during curing with a heating rate of 2 K/min and to determine the ceramic yield with a heating rate of 5 K/min (STA 409, Netzsch-Gerätebau GmbH, Germany). The crystallization was investigated by pyrolysis of cured precursor specimens, the curing was performed at 260 °C for 4 h at a pressure of 20 bar. For pyrolysis, a heating and cooling rate of 300 K/h and a dwell of 10 h at the target temperature were applied. The maximum temperatures were varied from 1100 °C to 1700 °C in 100 °C steps. Afterwards all samples were ground in a mixing mill (MM40, Retsch GmbH, Germany). The resulting density was determined by helium gas pycnometry (AccuPyc II 1340, Micromeritics Instrument Corporation, USA) and crystallization was monitored by XRD measurements (D8 Advance, Bruker Corporation,

Table 1
properties of SiC and C fibers as provided by manufacturers.

Fiber type		SiC	SiC	C (PAN)	C (Pitch)
Manufacturer		Tyranno ZMI Ube Industries Ltd.	Tyranno SA3 Ube Industries Ltd.	T800H Toray Industries Inc.	XN-90-60s Nippon Graphite Fiber Co.
Diameter	µm	11	7.5	5	10
Filaments	fil./yarn	800	1600	6000	6000
Tensile modulus	GPa	195	380	294	860
Tensile strength	MPa	3400	2400	5490	3430
Elongation	%	1.7	0.7	1.9	0.4
Density	g/cm^3	2.48	3.1	1.81	2.19
CTE	$10^{-6}/K$	4.0 (RT-1000)	4.5 (RT-1000)	−0.56	−1.5
Thermal conductivity	W/mK	2.5	65	35.1	500
Surface		smooth	rough	rutted	smooth

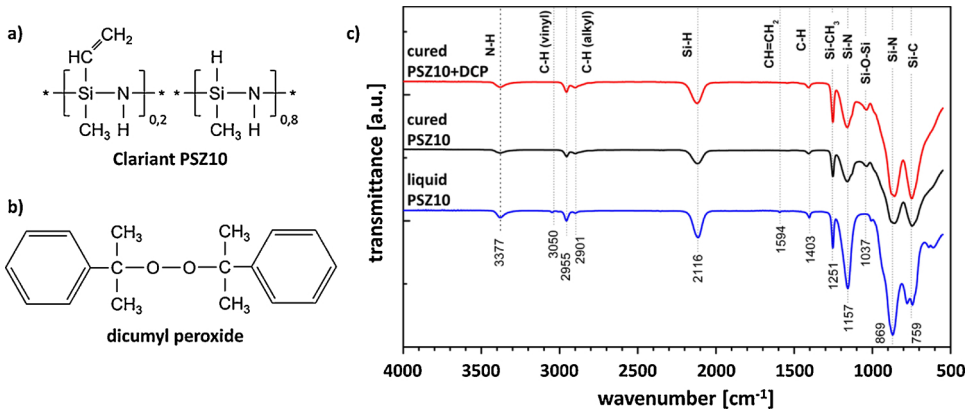

Fig. 2. Structural formula of the Clariant PSZ10 and dicumyl peroxide and corresponding infrared spectra of liquid PSZ10, and cured PSZ10 with and without 1 m.-% dicumyl peroxide as additive.

Germany) from 2θ = 10-90° with a step size of 0.01° and scanning time per step of 10 s).

3. Results and discussion

3.1. Characterization of the matrix precursor

The viscosity was measured in dependence of temperature with a heating rate of 2 K/min (Fig. 3a). At 25 °C, the viscosity of the polysilazane PSZ10 was 188 mPa·s and kept stable in the range of 170 and 190 mPa·s. The curing started at 131 °C at which the viscosity increased rapidly by cross-linking of the polymer. Since the resin transfer into the fiber preform and subsequent curing is performed in closed molds, the actual curing behavior can differ from the pressureless rheology measurement. In order to simulate this, DSC measurements were made in fully closed capsules. It was found, that the curing temperature was shifted to 273 °C (Fig. 3b) indicating, that a confined gas pressure in the capsules prevents the curing process. The curing reaction is suppressed and shifted towards higher temperatures. This was investigated further by TGA with a temperature program which was laid out in order to simulate a RTM cycle with a maximum temperature of 260 °C. The measurement confirmed that a drastic mass loss occurs above 120 °C (Fig. 3c). When reaching the maximum temperature, the PSZ10 already had a mass loss of over 4 wt.-%. This mass loss was also measured with

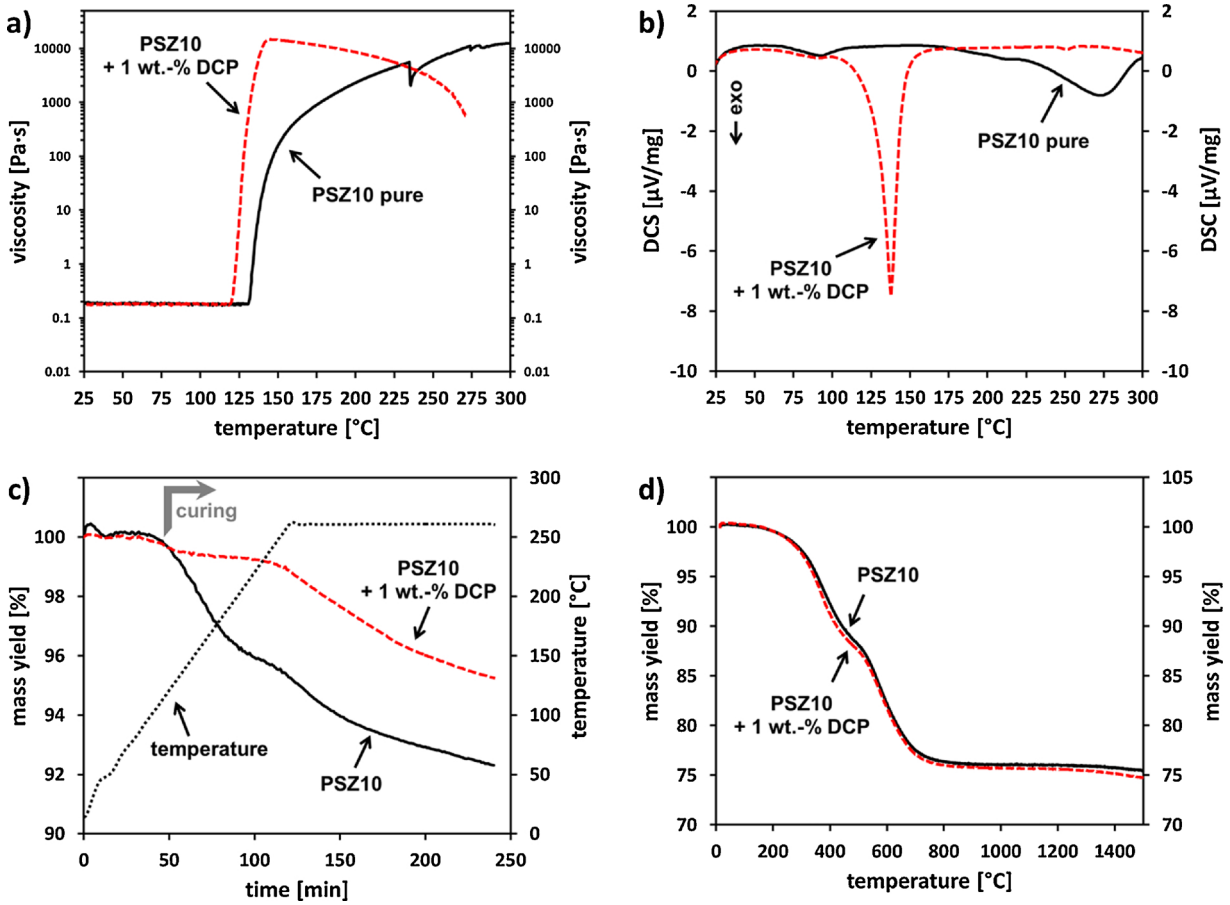

Fig. 3. Characterization of the PSZ10 polysilazane with and without dicumyl peroxide: a) viscosity; b) DSC; c) mass loss during curing; d) mass loss of the cured PSZ10 in nitrogen atmosphere.

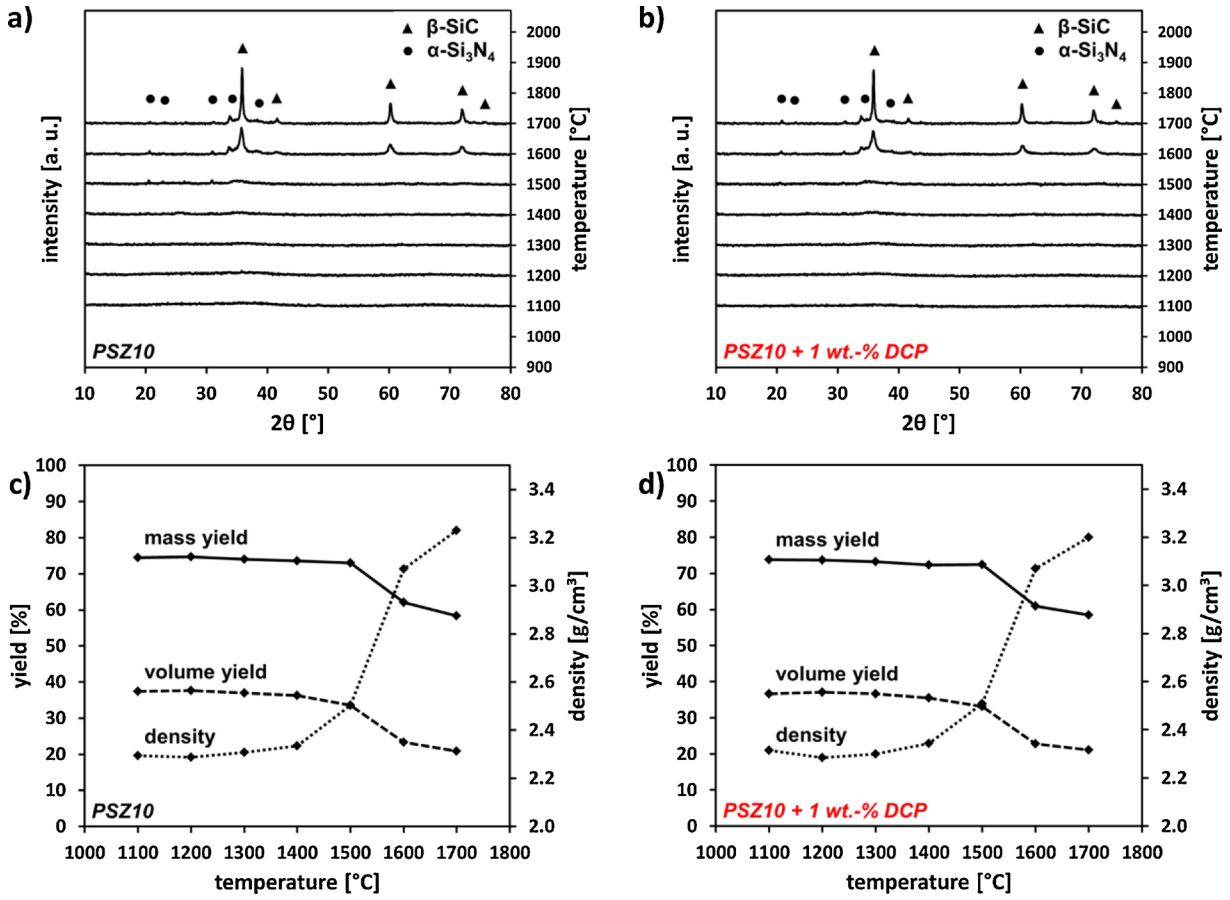

Fig. 4. Characterization of the PSZ10 polysilazane with and without dicumyl peroxide. Crystallization of PSZ10 and PSZ10 + dicumyl peroxide (a) and (b). Mass yield, volume yield and density of PZZ10 and PSZ10 + dicumyl peroxide (c) and (d).

other polysilazanes before and was associated with the evaporation of low molecular weight oligomers [16]. Nevertheless, polysilazanes can crosslink by transamination and dehydrogenation reactions under release of ammonia and hydrogen, too.

As the PSZ10 was applied to the RTM process, it was found that the cured fiber/polysilazane composites exhibited undesirable large voids. In consequence, more PIP cycles would have to be applied in order to create low porosity CMCs. It can be assumed, that this is associated with the evaporation of gaseous specimens, too. In order to overcome this effect by connecting smaller molecules with larger ones or with each other, and to promote the mass loss free hydrosilylation reaction via vinyl groups, the effect of dicumyl peroxide (DCP) was investigated. As can be seen from Fig. 2c, the crosslinking agent DCP considerably reduces the mass loss. The addition of DCP had no effect on the viscosity but decreased the curing temperature to 121 °C. In addition, the DSC measurement showed a crosslinking peak which now correlates better with the rheology measurement with a sharp maximum at 138 °C. The TGA measurements of both cured systems showed a similar behavior (Fig. 3d).

The molecular structure of PSZ10 was investigated in the liquid and cured state with and without DCP by means of infrared spectroscopy (Fig. 2c). In general, the spectra do not differ much. A small difference can be seen regarding the signal for the vinyl groups. Although it is low in the liquid sample, it is even lower in both cured samples. This leads to the assumption that the vinyl groups participate in both cases in the crosslinking mechanism. The cured samples showed the presence of Si-O-Si bonds indicating a certain degree of hydrolysis of the polysilazene during curing.

The crystallization for both systems also behaves similar. Fig. 4a and b shows the diffractograms of pure PSZ10 and PSZ10 + DCP which were pyrolyzed at temperatures from 1100 °C to 1700 °C. With increasing temperature the ceramic converts from fully X-ray amorphous to a more and more crystalline composition of Si_3N_4 and SiC. The polysilazane keeps X-ray amorphous at temperatures of up to 1400 °C. At 1500 °C the crystallization of α-Si_3N_4 was detected. Above 1500 °C, the presence of β-SiC was analyzed, too. The intensities for Si_3N_4 and SiC reach a maximum at the highest chosen temperature. With increasing crystallinity of the SiCN ceramics an increasing density was expected. Fig. 4c and Table 2 show the measured ceramic yields and densities of SiCN in dependence of temperature. All values are based on liquid PSZ10 with a density of 1.03 g/cm³. The volume yield can be calculated with the mass yield, the density of the polymer ρ_{poly} and the density of the pyrolyzed polymer ρ_{pyro} as follows:

$$Volume\ Yield = Mass\ Yield * \frac{\rho_{poly}}{\rho_{pyro}}$$

The density of pure PSZ10 pyrolyzed at 1100 °C was analyzed to be 2.29 g/cm³ and increased to 3.20 g/cm³ after annealing at 1700 °C. From 1100 °C to 1400 °C the increase in density is rather low. Above 1500 °C the density increases considerably faster due to the crystallization of SiC and Si_3N_4. At the same time the mass yield reduces by one third. The crystallization as well as the mass loss is associated with a carbothermal reduction occurring at temperatures above 1484 °C whereby free carbon is removed [22]:

$$Si_3N_4(s) + 3C(s) \rightarrow 3SiC\ (s) + 2N_2(g)$$

The measured density at 1700 °C was close to that of pure SiC

Table 2
Summary of the measured densities and calculated mass yields and volume yields of PSZ10. The values are based on the density of the as-received precursor.

temperature [°C]	Density PSZ10 [g/cm³]	mass yield PSZ10 [%]	vol. yield PSZ10 [%]	Density PSZ10 + DCP [g/cm³]	mass yield PSZ10 + DCP [%]	vol. yield PSZ10 + DCP [%]
as-received	1.03	–	–	1.03	–	–
260	1.15	93.4	83.7	1.15	94.0	84.2
1100	2.29	69.8	31.3	2.31	69.4	30.9
1200	2.29	69.8	31.4	2.28	69.4	31.3
1300	2.31	69.4	31.0	2.30	68.8	30.8
1400	2.33	68.7	30.3	2.34	68.0	29.9
1500	2.50	68.3	28.1	2.51	68.2	28.0
1600	3.07	57.9	19.4	3.07	57.2	19.2
1700	3.20	54.5	17.4	3.19	55.0	17.7

Table 3
Fiber volume contents (FVC) and mechanical properties of the manufactured composites.

Composite	FVC [%]	σ tensile [MPa]	E tensile [GPa]	ε tensile [%]
ZMI/SiCN	48	206 (± 79)	145 (± 3)	0.14 (± 0.05)
ZMI/SiCN oxid.	48	134 (± 18)	148 (± 3)	0.09 (± 0.01)
ZMI/SiCN CVD-SiC	48	239 (± 59)	168 (± 44)	0.17 (± 0.06)
ZMI/SiCN CVD-SiC oxid.	48	185 (± 49)	173 (± 16)	0.13 (± 0.06)
SA3/SiCN	45	478 (± 85)	206 (± 7)	0.26 (± 0.02)
SA3/SiCN oxid.	45	271 (± 62)	209 (± 12)	0.16 (± 0.06)
SA3/SiCN CVD-SiC	45	520 (± 79)	262 (± 49)	0.23 (± 0.05)
SA3/SiCN CVD-SiC oxid.	45	433 (± 89)	226 (± 35)	0.22 (± 0.03)
T800 H/SiCN	46	224 (± 40)	182 (± 10)	0.13 (± 0.03)
T800 H/SiCN oxid.	46	–	–	–
T800 H/SiCN CVD-SiC	46	254 (± 26)	159 (± 14)	0.19 (± 0.02)
T800 H/SiCN CVD-SiC oxid.	46	226 (± 17)	124 (± 18)	0.20 (± 0.02)
XN90/SiCN	42	288 (± 39)	275 (± 22)	0.12 (± 0.03)
XN90/SiCN oxid.	42	4 (± 3)	67 (± 27)	0.01 (± 0.01)
XN90/SiCN CVD-SiC	42	384 (± 47)	226 (± 20)	0.19 (± 0.03)
XN90/SiCN CVD-SiC oxid.	42	283 (± 24)	209 (± 17)	0.20 (± 0.01)

(3.21 g/cm³) and Si_3N_4 (3.18 g/cm³) [23]. At the highest temperature the volume yield was only 17.4% which is nearly half of the volume yield measured at 1100 °C (Table 2). The DCP showed negligible effects on crystallization and densities (Fig. 4b and d).

3.2. Preparation of the composites

The four chosen types of fibers were unidirectionally wound on graphite mandrels (Fig. 1). The preform with XN90 fibers showed a considerable amount of damage, especially on the curved edges of the mandrel. This can be associated with the high modulus and low fracture strain rates of the fibers. No visual fiber damage was seen with the other types. Due to improved results with the curing agent DCP, all composites were infiltrated with the PSZ10-DCP mixture. For a low cost PIP process an amorphous matrix is favorable. A crystallized SiCN matrix has a low volume yield which leads to a high amount of porosity after each PIP cycle. This will in turn lead to more infiltration cycles to manufacture low porosity composites. Nevertheless, in order to produce composites for applications at temperatures of up to 1200 °C, a higher pyrolysis temperature of 1300 °C was applied. The resulting fiber volume contents are listed in Table 3. The determined values were similar except for that of the XN90 fiber based composite with a slightly higher porosity and lower fiber volume content. The porosities for the ZMI, SA3, T800H and XN90 composites were measured to amount 5.6, 6.0, 6.1 and 8.1 vol.-%, respectively.

3.3. Characterization of the CMCs

A total of 80 samples were prepared for tensile tests of which half were equipped with an additional CVD-SiC coating. The coating had a thickness of 70–100 µm. Thereof 20 coated and 20 uncoated samples were oxidized in air at 1200 °C for 10 h. An overview over the results is given in Table 3 and Fig. 5a.

The tensile tests showed that the resulting mechanical properties are highly dependent of the type of fiber. Nevertheless, there is a strong deviation between the single fiber properties and the composite properties. Only the Young's moduli of the composites correlate with those of the single fibers. The tensile strength as well as the fracture strain do not correlate at all. The highest strength with 478 MPa was achieved with the Tyranno SA3-based composite, although the single fiber strength is only 2400 MPa. In comparison, the T800H-based composite had a tensile strength of 224 MPa, while the single fiber strength amounts 5490 MPa, which is more than twice of that of the SA3. This behavior is similar with the fracture strain. The SA3-based composite had a fracture strain of 0.26%, the T800H based composite only half of that. The single fiber fracture strain in comparison is 0.7 and 1.9%, respectively. The composite with the ZMI fiber had the lowest strength with 206 MPa. The XN90 based composite revealed a strength of 288 MPa, which is the second highest value of the four composites. After oxidation at 1200 °C, the SiC fiber based composites showed a substantial decrease in strength and fracture strain. The Young's moduli kept similar. The carbon fiber based composites exhibited a highly brittle behavior after oxidation and most samples broke during the mounting in the tensile testing machine. The experiments were repeated with samples covered by a CVD-SiC coating. Composites with coating had a slightly higher strength compared to those without coating. After oxidation, a certain decrease in strength was analyzed, nevertheless this decrease was substantially lower than that for samples without coating. The Young's moduli showed similar values.

For a better comparison of the performance of the different type of fibers, the fiber strength utilization (FSU) is calculated. The formula includes the composite tensile strength σ_{comp}, the single fiber tensile strength σ_{fiber} and the fiber volume content (FVC) and is calculated as follows:

$$FSU = \frac{\sigma comp}{\sigma fiber \cdot FVC}$$

The FSU values for the ZMI and T800H based composites are low. Those for the SA3 are the highest, those for the XN90 are in between (Fig. 5b). Several reasons for the different FSU values can be taken into account. First of all, there is little knowledge about the damage resulting from the winding process. From the visual impression, the XN90 fibers showed damaging. Another question is if the manufacturing process has an influence on the degradation of fibers. In general, PIP is a rather soft infiltration technique. During curing and pyrolysis the polymer decomposes under the release of NH_3, CH_4 and H_2 [16]. The degassing is completed at a temperature of 700 °C (Fig. 3d). A reaction of the fibers with the released volatile compounds is rather unlikely and is not considered in our study. The maximum annealing temperature was 1300 °C. This temperature is lower than that of the manufacturing temperature of the SA3 and the XN90 but in the same range of the ZMI

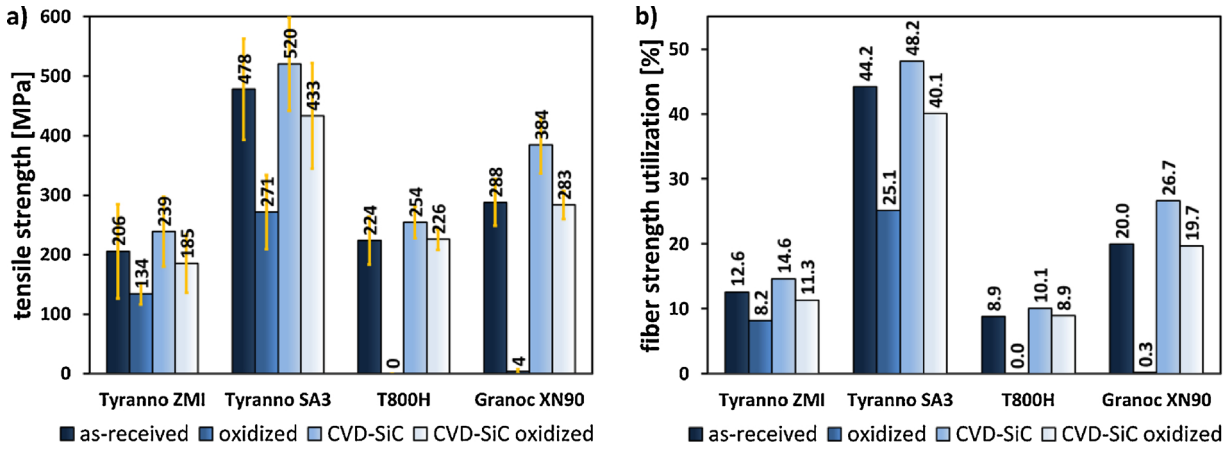

Fig. 5. Comparison of the tensile strengths of the four CMCs: a) tensile strength of unoxidized and oxidized samples, with and without CVD-SiC coating; b) fiber strength utilization of the CMCs.

and PAN-based carbon fibers [24,25]. Due to the similar temperature of that of the pyrolysis process, a thermal degradation of these two fibers might be possible. In previous research it was found that ZMI based SiCN composites that were pyrolyzed at only 1000 °C exhibited a similar, brittle fracture behavior [26]. In conclusion, the applied 1300 °C is rather unlikely to be the crucial factor for the low mechanical properties of the ZMI. Unfortunately, there is no data concerning the properties of T800 H/SiCN composites that were manufactured at lower temperatures. Nevertheless, this was done with another PAN based carbon fiber (Toho Tenax HTA). HTA/SiCN composites that were pyrolyzed at 1000 °C showed low tensile strengths, too [27]. Apparently, there is also no correlation between the fiber roughness (Table 1) and the fiber strength utilization. The ZMI and the XN90 both have a smooth surface while the SA3 and the T800H are rough. There might be the possibility of a chemical interlocking of the fiber and the matrix in some cases since all fibers have a different microstructure and chemical composition. The SA3 and the XN90 consist of SiC crystals and graphite, respectively. The SA3 fiber is basically free of oxygen, especially on the outside [28] while the ZMI fiber is amorphous and oxygen rich [24]. Carbon fibers typically obtain an oxidative surface treatment and a sizing for their typical usage in CFRP composites [29]. For PAN and pitch based fibers it was shown, that the surface composition has a strong influence on wetting properties [30,31]. Little is known about the wetting and reactivity of polysilazanes with the four chosen fibers.

In previous research, it was found that SiC fabric based SiCN composites exhibit pore channels which are oriented parallel to the fiber direction. For a 2D fiber orientation, the resulting pore channels were oriented in the same 2D directions [17]. CT scans showed that the porosity in the manufactured UD composites is oriented parallel to the fiber bundles, too. Rarely, no porosity was analyzed perpendicular to the fibers. The porosity occurred in form of long, thin channels. No huge differences regarding the pore morphologies were analyzed. After oxidation at 1200 °C for 10 h, the porosity did not change for the SiC-fiber based composites. However, the carbon fiber based composites showed a huge increase of porosity as can be seen in the µCT scans due to the oxidation of the fibers (Fig. 6). In the samples without protective CVD-SiC coating the atmospheric oxygen could easily burn out the fibers and proceed in the newly formed cavities.

SEM micrographs showed that all composites had a dense microstructure (Figs. 7 and 8). Nevertheless, some thin gaps in the matrix and on some fiber/matrix interfaces were found. A degradation of the fibers or a reaction with the matrix was not detected. The matrix showed a layered structure, parallel to the fiber surfaces. This was created during pyrolysis, when the polysilazane shrunk off the fiber towards the space between fibers. Every PIP cycle added a new layer of SiCN until the gap between fiber and matrix was not apparent any more. This effect was already reported with other polysilazanes [32]. Nevertheless, especially the SiC fiber based composites showed some residual gaps, which were typically oriented perpendicular to the fiber surface.

As can be seen from Fig. 8, SiCN was found within the XN90 fibers. Presumably, the core of the fibers was hollow and infiltrated with the polysilazane. Some of the fibers exhibited a rupture from the edge towards the core. Since substantial fiber damage was observed after winding, the polysilazane had access to the hollow core. SEM images of fractured surfaces revealed that the SA3 and XN90 based composites exhibited a huge fiber pullout. In comparison, the fiber pullout of the ZMI and T800H based composites was rather small. This is in good agreement with the fiber strength utilization values. From SEM images the pullout of the XN90 fibers appeared to be the strongest of all fibers, but the fiber strength utilization is lower compared to the SA3. This behavior has to be discussed in terms of the fiber damage after winding.

Besides a potential degradation of the fibers, an explanation for the different FSU values has to be discussed in terms of weak interface (WIC) and weak matrix composites (WMC). Non brittle behavior is achieved if either the crack resistance of the fiber matrix interface is low enough to ensure a debonding between fiber and matrix (WIC) or the matrix strength is low enough to induce multiple cracking while the fibers remain intact (WMC). As can be seen from Fig. 7, the fiber/matrix interfaces of all four fiber types are similar. Hence, all composites are expected to show a comparable fiber-pullout behavior. However, this was not the case.

Brittle and non-brittle behavior is dependent from the relative fracture energy of the interface and fiber as well as the relative Young's modulus ratio of the fiber and matrix [33,34]. The higher the relative Young's modulus ratio, the more likely the composite can function as WMC, comparable to carbon/carbon and oxide/oxide, which can be estimated by calculations. The Young's modulus was not determined for PSZ10 derived SiCN but for other polymer derived ceramics [35]. The Young's moduli of a comparable polyureamethylvinylsilazane derived SiCN were in the range of 82–140 GPa [36]. The relative Young's moduli $[(E_{fiber}\text{-}E_{matrix})/(E_{fiber}+E_{matrix})]$ were calculated with the mean value of the SiCN modulus of E_{matrix} = 111 GPa. For the ZMI, SA3, T800H and XN90 the results were 0.27, 0.55, 0.45, 0.77, respectively. The values for the SA3 and XN90 are the highest, those of the ZMI and T800H are the lowest. This is in good agreement with the seen fiber pullout, indicating that the SA3/SiCN and XN90/SiCN composites have to be considered as weak matrix composites.

After oxidation, the fractured surfaces showed a highly brittle behavior. Within all carbon fiber based composites the fibers were completely removed by the oxidation causing highly porous structures. In case of the XN90 based composites the SiCN cores remained intact. The SiC fiber based composites remained dense but the fiber pullout was

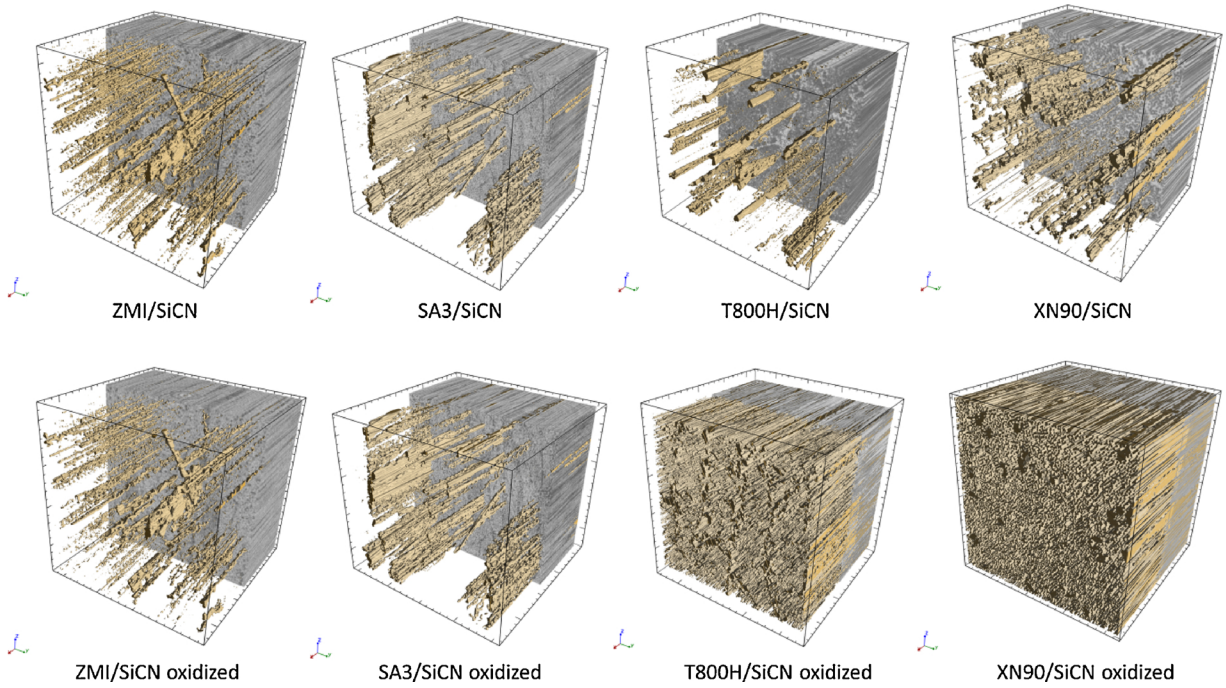

Fig. 6. 3D-µCT illustrations of representative sections of the investigated composites with dimensions of 1 × 1x1 mm^3 before and after oxidation. The front parts of the illustrations were cut out and the porosity was highlighted to visualize the pore channels.

reduced. Interestingly, in case of the SA3 based composite, only the edges of the tensile samples showed a brittle behavior, the core remained damage tolerant. Presumably a longer oxidation time would have caused an embrittlement of the core. In case of the CVD-SiC coated, oxidized samples the microstructures remained similar compared to that of the native samples.

The interfaces of the SiC fiber based composites were investigated in more detail by means of EDX. Some thin gaps were found in the matrix perpendicular to the fibers (Figs. 9 and 10a). The mappings showed that the interfaces between single PIP cycles as well as between fibers and matrix exhibit oxygen, while the rest of the SiCN matrix is rather free of oxygen. At the PIP- and fiber/matrix interfaces oxygen concentrations of approximately 5–10 and 20 at.-% were detected. It is assumed that this finding is due to the handling of the CMCs in air. In the past, the release of ammonia was detected when SiCN based CMCs pyrolyzed at lower temperatures were handled in air. This can be associated with a

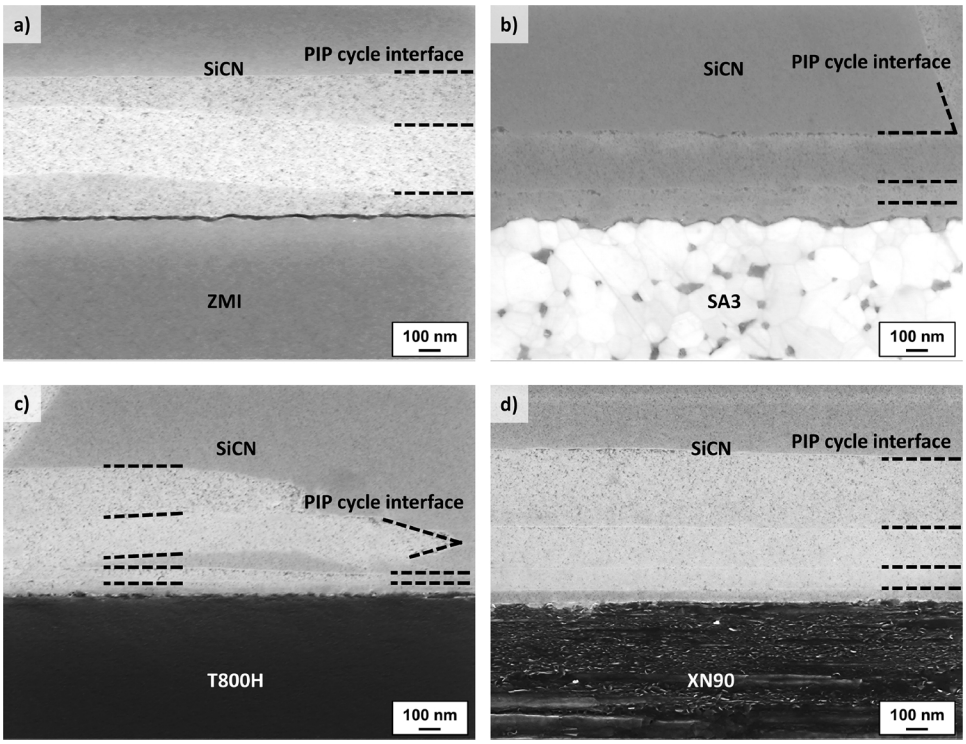

Fig. 7. Fiber/matrix bonding of the four composites. The fibers are oriented horizontally: a) ZMI/SiCN; b) SA3/SiCN; c) T800H/SiCN; d) XN90/SiCN.

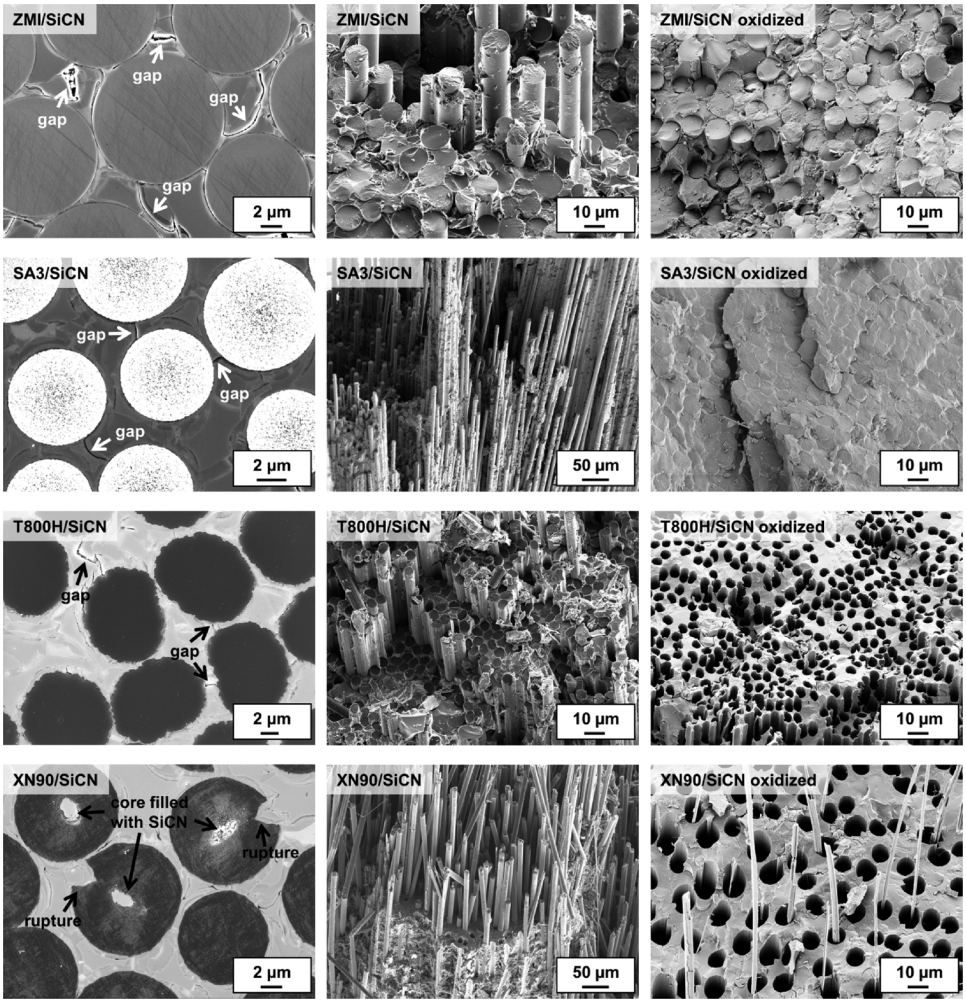

Fig. 8. SEM images of polished cross-sections and fractured surfaces after manufacturing in comparison to fractured surfaces after oxidation.

hydrolysis reaction of SiCN surfaces. Although this effect was tremendously reduced by the chosen temperature of 1300 °C, a slight release of ammonia was still detected. In consequence, any new PIP cycle added a thin layer of oxygen enriched SiCN. As shown in Fig. 7, the density of the layers is high close to the fiber surface. After oxidation, the oxygen content increased to 20–40 and 40–50 at.-%, respectively, while the oxygen content in the rest of the matrix and inside the fibers remained low. Any SiCN/SiCN-interfaces were not distinguishable any more. In addition, pores were created at the interfaces (Figs. 9 and 10b). It seems that the gaps and SiCN/SiCN-interfaces are pathways for the transport of oxygen into the composites. Since the amount of SiCN/SiCN-interfaces is high close to the fiber surface, the oxygen is enriched mostly here. Possibly these gaps and interfaces weaken the matrix by providing planes for crack propagation and thereby help the material to function as WMC. Their oxidation might lead to a strengthening of the matrix and in turn would affect the mechanisms of weak matrix composites. In addition, the enrichment of oxygen close to the fiber surface might have resulted in an oxidative interlocking.

4. Conclusion

An organopolysilazane was investigated with regard to its applicability for the polymer infiltration and pyrolysis process. It was found that the polysilazane has a favorable low viscosity and high mass yield. At temperatures above 1400 °C, the amorphous SiCN ceramic starts to crystallize. At 1700 °C, the density of the ceramic reached a maximum of 3.20 g/cm^3 which is close to that of the density of pure SiC and Si_3N_4. The polysilazane was used to manufacture four different unidirectionally fiber reinforced ceramic matrix composites without fiber coating. It was found that the addition of dicumyl peroxide helps to improve the infiltration results. Depending on the type of fiber, different tensile strengths were obtained. The composites with the Tyranno SA3 fiber and the pitch based Granoc XN90 fiber had the highest tensile strengths of 478 and 288 MPa, respectively. Both composites exhibited a strong fiber pullout performance, whereas the composites with the Tyranno ZMI and T800H fibers resulted in a brittle fracture behavior. Regarding the fiber strength utilization, the differences between the composites were even more pronounced. Especially composites with pitch based fibers might be an interesting research topic, due to the excellent fiber pullout. Nevertheless, the occurred damage of the fibers during preforming has to be reduced in future in order to increase the strength.

The synergistic effect of high fiber modulus and low matrix modulus is assumed to be the reason for the different mechanical properties. The composites containing the high modulus SA3 and XN90 fibers with the low modulus SiCN matrix create weak matrix composites. The PIP related gaps in the matrix as well as the high amount of SiCN/SiCN interfaces, especially close to the fiber surfaces weaken the matrix even more. Besides the weak matrix theory, other factors such as chemical composition, crystallinity and surface roughness of the fibers have an influence on the fiber-matrix bonding and explain the different mechanical properties. Hence, for a satisfying verification of this theory,

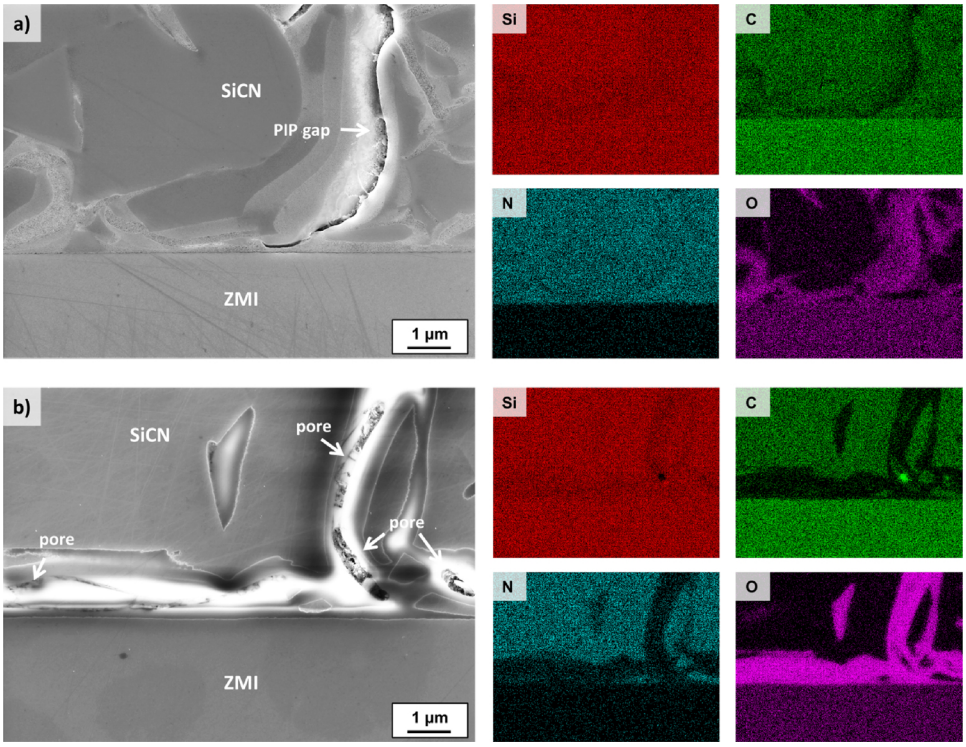

Fig. 9. EDX analysis of representative ZMI/SiCN interfaces: a) non-oxidized interface; b) oxidized interface.

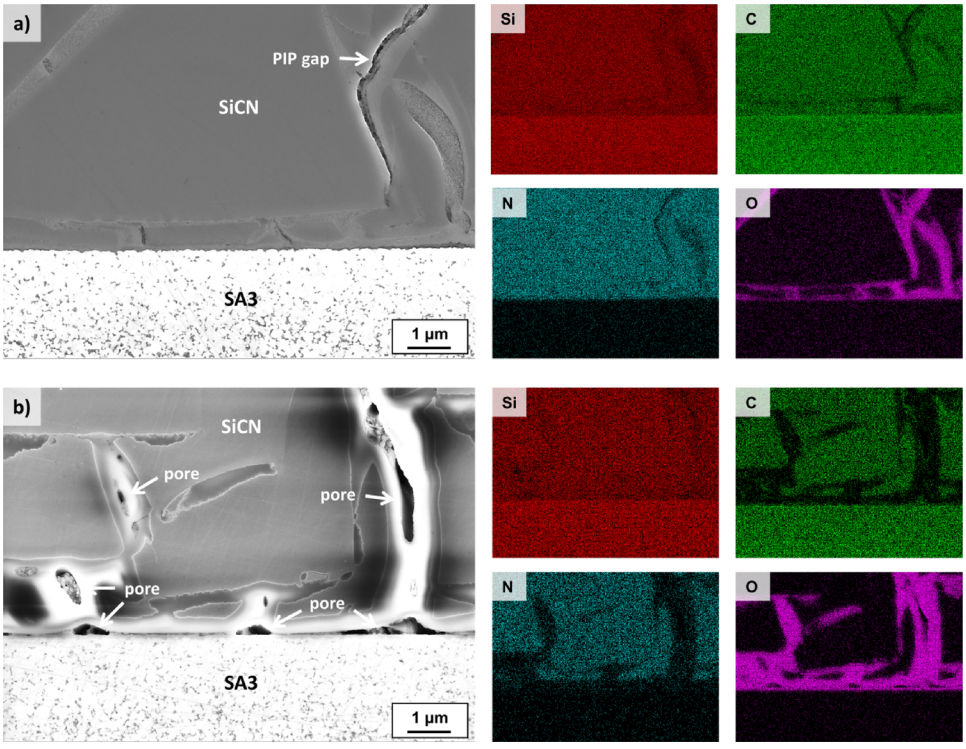

Fig. 10. EDX analysis of representative SA3/SiCN interfaces: a) non-oxidized interface; b) oxidized interface.

composites with fibers of identical chemical composition and surfaces but with different Young's moduli should be manufactured and compared.

Oxidation tests at 1200 °C for 10 h revealed, that especially the carbon fiber reinforced composites degrade quite severe, resulting in high brittleness. The SiC fiber based composites did not degrade that severe but exhibited a significant loss in strength and fracture strain. It was detected that pore surfaces generated by the PIP process as well as the SiCN/SiCN interfaces were strongly oxidized. Their oxidation leads to a strengthening of the matrix and in turn would affect the mechanism of weak matrix composites. In addition, these interfaces act as pathways for oxygen diffusing towards the fiber surface resulting in an oxidative interlocking of the fibers with the matrix.

Acknowledgements

The financial support for the NewAccess project (03EK3544) by the Bundesministerium für Bildung und Forschung (Germany) is gratefully acknowledged.

References

[1] N.P. Padture, Advanced structural ceramics in aerospace propulsion, Nat. Mater. 15 (2016) 804–809.
[2] S. Wu, L. Cheng, L. Zhang, Y. Xu, Thermal shock behavior of a three-dimensional SiC/SiC composite, Metall. Mater. Trans. A 37 (12) (2006) 3587–3592.
[3] S. Guo, Y. Kagawa, Tensile fracture behavior of continuous SiC fiber-reinforced SiC matrix composites at elevated temperatures and correlation to in situ constituent properties, J. Eur. Ceram. Soc. 22 (13) (2002) 2349–2356.
[4] F. Breede, S. Hofmann, N. Jain, R. Jemmali, Design, manufacture, and characterization of a carbon fiber-reinforced silicon carbide nozzle extension, Int. J. Appl. Ceram. Technol. 13 (1) (2016) 3–16.
[5] W. Krenkel, Carbon fibre reinforced silicon carbide composites (C/SiC, C/C-SiC), in: N.P. Bansal (Ed.), Handbook of Ceramic Composites, Springer US, Boston, MA, 2005, pp. 117–148.
[6] W. Krenkel, F. Berndt, C/C–SiC composites for space applications and advanced friction systems, Mater. Sci. Eng. A 412 (1-2) (2005) 177–181.
[7] G. Corman, K. Luthra, J. Jonkowski, J. Mavec, P. Bakke, D. Haught, Melt Infiltrated Ceramic Matrix Composites for Shrouds and Combustor Liners of Advanced Industrial Gas Turbines – Advanced Materials for Advanced Industrial Gas Turbines (AMAIGT) Program Final Report, Department of Energy, United States, 2011.
[8] G.S. Corman, K.L. Luthra, Silicon melt infiltrated ceramic composites (HiPerComp™), in: N.P. Bansal (Ed.), Handbook of Ceramic Composites, Springer US, Boston, MA, 2005, pp. 99–115.
[9] Y. Katoh, M. Kotani, H. Kishimoto, W. Yang, A. Kohyama, Properties and radiation effects in high-temperature pyrolyzed PIP-SiC/SiC, J. Nucl. Mater. 289 (1) (2001) 42–47.
[10] C.A. Lewinsohn, C.H. Henager, G.E. Youngblood, R.H. Jones, E. Lara-Curzio, R. Scholz, Failure mechanisms in continuous-fiber ceramic composites in fusion energy environments, J. Nucl. Mater. 289 (1) (2001) 10–15.
[11] M.A. Snead, Y. Katoh, T. Koyanagi, G.P. Singh, SiC/SiC Cladding Materials Properties Handbook, Oak Ridge National Lab. (ORNL), Oak Ridge, TN (United States), 2017 p. Medium: ED; Size: 55 p..
[12] S. Bertrand, O. Boisron, R. Pailler, J. Lamon, R.R. Naslain, (PyC/SiC)n and (BN/SiC)n nanoscale-multilayered interphases by pressure pulsed-CVI, Key Eng. Mater. 164 (165) (1999) 357–360.
[13] S. Bertrand, C. Droillard, R. Pailler, X. Bourrat, R. Naslain, TEM structure of (PyC/SiC)n multilayered interphases in SiC/SiC composites, J. Eur. Ceram. Soc. 20 (1) (2000) 1–13.
[14] R. Naslain, O. Dugne, A. Guette, J. Sevely, C.R. Brosse, J.P. Rocher, J. Cotteret, Boron nitride interphase in ceramic-matrix composites, J. Am. Ceram. Soc. 74 (10) (1991) 2482–2488.
[15] C. Sauder, A. Brusson, J. Lamon, Influence of interface characteristics on the mechanical properties of Hi-nicalon type-S or tyranno-SA3 fiber-reinforced SiC/SiC minicomposites, Int. J. Appl. Ceram. Technol. 7 (3) (2010) 291–303.
[16] G. Motz, S. Schmidt, S. Beyer, The PIP-process: precursor properties and applications, Ceramic Matrix Composites, Wiley-VCH Verlag GmbH & Co. KGaA, 2008, pp. 165–186.
[17] B. Mainzer, M. Friess, R. Jemmali, D. Koch, Development of polyvinylsilazane-derived ceramic matrix composites based on Tyranno SA3 fibers, J. Ceram. Soc. Jpn. 124 (10) (2016) 1035–1041.
[18] R. Riedel, M. Seher, J. Mayer, D.V. Szabó, Polymer-derived Si-based bulk ceramics, part I: preparation, processing and properties, J. Eur. Ceram. Soc. 15 (8) (1995) 703–715.
[19] E. Ionescu, Polymer-derived ceramics, Ceramics Science and Technology, Wiley-VCH Verlag GmbH & Co. KGaA, 2012, pp. 457–500.
[20] M. Bouchez, M. Axtmann, C. Davoine, M. Kuhn, C. Wilhemi, J.-F. Justin, V. Fernandez Villace, E. Dufour, J.R. Riccius, Combustor Materials Research Studies for High Speed Aircraft in the European Program ATLLAS2, 20th AIAA International Space Planes and Hypersonic Systems and Technologies Conference (2015).
[21] H.J. Seifert, S. Wagner, O. Fabrichnaya, H.L. Lukas, F. Aldinger, T. Ullmann, M. Schmucker, H. Schneider, Yttrium silicate coatings on chemical vapor deposition-SiC-precoated C/C-SiC: thermodynamic assessment and high-temperature investigation, J. Am. Ceram. Soc. 88 (2) (2005) 424–430.
[22] H.J. Seifert, J. Peng, H.L. Lukas, F. Aldinger, Phase equilibria and thermal analysis of Si–C–N ceramics, J. Alloys. Compd. 320 (2) (2001) 251–261.
[23] M. Srinivasan, W. Rafaniello, Non-oxide materials: applications and engineering, in: A.W. Weimer (Ed.), Carbide, Nitride and Boride Materials Synthesis and Processing, Springer Netherlands, Dordrecht, 1997, pp. 3–42.
[24] J.A. DiCarlo, H.-M. Yun, Non-oxide (silicon carbide) fibers, in: N.P. Bansal (Ed.), Handbook of Ceramic Composites, Springer, US, Boston, MA, 2005, pp. 33–52.
[25] B.A. Newcomb, Processing, structure, and properties of carbon fibers, Compos. Part A Appl. Sci. Manuf. 91 (2016) 262–282.
[26] E. Daenicke, Entwicklung hochtemperaturbeständiger keramischer Faserverbundwerkstoffe auf der Basis von SiC- und neuartigen SiBNC-Fasern, PhD Thesis, DLR, Bibliotheks- und Informationswesen, Köln, 2014, p. 238.
[27] G. Stantschev, M. Frieß, R. Kochendörfer, W. Krenkel, Long fibre reinforced ceramics with active fillers and a modified intra-matrix bond based on the LPI process, J. Eur. Ceram. Soc. 25 (2-3) (2005) 205–209.
[28] E. Buet, C. Sauder, S. Poissonnet, P. Brender, R. Gadiou, C. Vix-Guterl, Influence of chemical and physical properties of the last generation of silicon carbide fibres on the mechanical behaviour of SiC/SiC composite, J. Eur. Ceram. Soc. 32 (3) (2012) 547–557.
[29] U. Zielke, K.J. Hüttinger, W.P. Hoffman, Surface-oxidized carbon fibers: I. Surface structure and chemistry, Carbon 34 (8) (1996) 983–998.
[30] A. Martin, F. Addiego, G. Mertz, J. Bardon, D. Ruch, P. Dubois, Pitch-based carbon fibre-reinforced peek composites: optimization of interphase properties by water-based treatments and self-assembly, J. Mater. Sci. Eng. 05 (06) (2016).
[31] J. Xie, D. Xin, H. Cao, C. Wang, Y. Zhao, L. Yao, F. Ji, Y. Qiu, Improving carbon fiber adhesion to polyimide with atmospheric pressure plasma treatment, Surf. Coat. Technol. 206 (2) (2011) 191–201.
[32] G. Ziegler, I. Richter, D. Suttor, Fiber-reinforced composites with polymer-derived matrix: processing, matrix formation and properties, Compos. Part A Appl. Sci. Manuf. 30 (4) (1999) 411–417.
[33] D. Koch, K. Tushtev, G. Grathwohl, Ceramic fiber composites: experimental analysis and modeling of mechanical properties, Compos. Sci. Technol. 68 (5) (2008) 1165–1172.
[34] D. Koch, Microstructural modeling and thermomechanical properties, in: W. Krenkel (Ed.), Ceramic Matrix Composites, WILEY-VCH Verlag GmbH & Co.KGaA, Weinheim, Germany, 2008.
[35] P. Colombo, G. Mera, R. Riedel, G.D. Soraru, Polymer-derived ceramics: 40 years of research and innovation in advanced ceramics, J. Am. Ceram. Soc. 93 (7) (2010) 1805–1837.
[36] N. Janakiraman, F. Aldinger, Fabrication and characterization of fully dense Si–C–N ceramics from a poly(ureamethylvinyl)silazane precursor, J. Eur. Ceram. Soc. 29 (1) (2009) 163–173.